STEMO, a Stabilized Toolkit for Embedded Dielectric Structures with MOment Methods

Emmanuel Van Lil[1], Jan-willem De Bleser[2]
[1] KU Leuven, div. ESAT/TELEMIC, B-3001 Heverlee, Belgium, Emmanuel.VanLil@ESAT.KULeuven.Be
[2] idem, but e-mail address Jan-willem.De.Bleser@JPL.NASA.gov

***Abstract*— The low frequency instability in the method of moments becomes important when objects smaller than the wavelength have to be computed. For a PEC (Perfectly Electrically Conducting) body, this leads to uncoupling or splitting the integral equations by using first the MFIE (Magnetic Field Integral Equation) for the currents and consecutively the EFIE (Electric Field Integral Equation) for the charges. For dielectric bodies, the charge is reintroduced. The contribution of this paper consists in implementing an efficient technique, reducing the computational complexity, in time but mostly in memory. A toolkit has been developed to perform accurate computations. The technique has been verified quantitatively, checking the charge and current distributions against analytic solutions where existing, as well as qualitatively against the boundary conditions for the scattered field. Many examples will be given, both in frequency and in time domain (obtained by inverting frequency domain calculations including the DC (Direct Current) component).**

***Index Terms*—Electromagnetic Field Integral equations, time domain, frequency domain, electrically small bodies.**

I. INTRODUCTION

The physical cause of the stability problem is the relationship, or rather the lack of relationship between charge (leading to the scalar potential) and current (leading to the vector potential) in electrostatics. To formulate the EFIE, the Lorenz gauge $\vec{\nabla}\bullet\vec{A}_e = -j\omega\mu\varepsilon\varphi_e$ is used to eliminate the scalar potential and hence the charge. One can see that, at low frequencies, the potential becomes so large, that the equations become numerically unstable. If we keep both electric potentials as well as their magnetic counterparts (for dielectric bodies), we can compute the EM (Electromagnetic) fields from those 4 unknown functions (2 scalar and 2 vectorial) as follows:

$$\begin{aligned}\vec{E} &= \vec{\nabla}\times\vec{A_m}/\varepsilon - \vec{\nabla}\varphi_e - j\omega\vec{A_e}\\ \vec{H} &= \vec{\nabla}\times\vec{A_e}/\mu + \vec{\nabla}\varphi_m + j\omega\vec{A_m}\end{aligned} \qquad (1)$$

If we find sufficient equations (through the application of the appropriate boundary conditions) to solve for all the unknown functions, those equations do not pose problems at low frequencies, as was already proposed by Taskinen and Oijala [1].

A. Need for stabilization

We should note that the combined or hybrid field integral equations, as proposed by Chew, Jin, Michielssen and Song [2] is not a solution to the problem, since the problem lies in the instability of the EFIE at low frequencies, even if it solves the problem of internal resonances for closed surfaces. We rewrite the expressions for the scalar and vector potentials as to obtain mathematically more similar expressions for all integrals, even if the physical meaning is somewhat lost. Assuming that only currents are presents on the surface between otherwise LHI (linear, homogeneous and isotropic) objects, numbered i, our potentials are defined as follows:

$$\begin{aligned}\vec{A}_{i,\left\{\substack{e\\m}\right\}}(\vec{r}) &= \oiint \vec{J}_{s,\left\{\substack{e\\m}\right\}}(\vec{r}\,')G_i(|\vec{r}-\vec{r}\,'|)dS'\\ \phi_{i,\left\{\substack{e\\m}\right\}}(\vec{r}) &= \oiint \rho_{s,\left\{\substack{e\\m}\right\}}(\vec{r}\,')G_i(|\vec{r}-\vec{r}\,'|)dS'\\ G_i(r) &= \frac{e^{-jk_i r}}{4\pi r}\end{aligned} \qquad (2)$$

B. Implementation of the stabilization

In those assumptions, we can now require that the incident fields match the fields produced by the surface currents so that the boundary conditions at all interfaces are satisfied. We assume a situation like in Fig. 1.

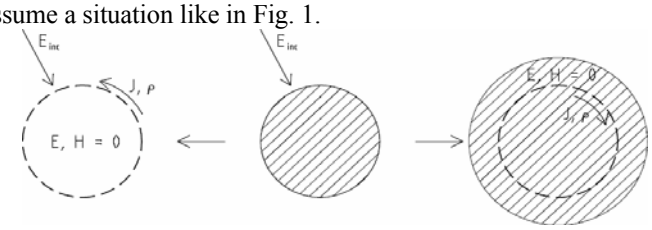

Fig. 1. Assumptions for a single object interface.

We note that this can be easily generalized for objects embedded in each other, so that we can go from layer i to layer i+1, until we are in the centre of the composite object.

This leads to the following set of equations for the case of an object i+1 immersed in object i (we assume that the excitation lies in medium i).

$$\begin{bmatrix} \vec{E}_{i,inc} \\ \vec{H}_{i,inc} \\ 0 \\ 0 \end{bmatrix} = \begin{bmatrix} \mu_i M_i^r & \frac{M_i^b}{\varepsilon_i} & M_i^c & 0 \\ M_i^c & 0 & -\varepsilon_i M_i^r & -\frac{M_i^b}{\mu_i} \\ \mu_{i+1} M_{i+1}^r & \frac{M_{i+1}^b}{\varepsilon_{i+1}} & M_{i+1}^c & 0 \\ M_{i+1}^c & 0 & -\varepsilon_{i+1} M_{i+1}^r & -\frac{M_{i+1}^b}{\mu_{i+1}} \end{bmatrix} \begin{bmatrix} \vec{J}_{s,e} \\ \rho_{s,e} \\ \vec{J}_{s,\mathrm{m}} \\ \rho_{s,\mathrm{m}} \end{bmatrix} \quad (3)$$

The charges and currents exist in this case on the surface of the interface between layer i and i+1. If we subdivide the surface in triangles, the minimum size of the matrix is 5nx5n. Of course we may impose more constraints than unknowns. We have shown in [3] that this might benefit the accuracy, without penalizing (too) much the computer time.

C. *Implementation of the toolkit*

The first part consists in meshing the object. This was done with a freeware mesher, gmsh [4]. For complex objects one has to make sure that the object is "watertight", in that sense that no gaps are left open on both sides of a boundary line. By expanding the currents and charges and testing them, we can derive the expressions of the matrices in (3).

$$\begin{aligned} M_i^r &= j\omega \iint \vec{g}(\vec{\mathrm{r}}) \cdot \vec{f}(\vec{\mathrm{r}}') G_i dS' dS \\ M_i^b &= \int \vec{g}(\vec{\mathrm{r}}) \cdot \delta\vec{n}(\vec{\mathrm{r}}) dS + \iint \vec{g}(\vec{\mathrm{r}}) \cdot \vec{\nabla}_r G_i \Pi(\vec{\mathrm{r}}') dS' dS \\ M_i^c &= \int \vec{g}(\vec{\mathrm{r}}) \cdot \delta\vec{f}(\vec{\mathrm{r}}) \times \vec{n}(\vec{\mathrm{r}}) dS - \iint \vec{\nabla}_r G_i \times \vec{f}(\vec{\mathrm{r}}') dS' dS \end{aligned} \quad (4)$$

$\vec{g}$ being the testing functions, $\vec{f}$ the expansion functions for the currents (in this case classical Rao Wilton Glisson (RWG) functions [5] were used), and Π the expansion functions for the charges. The first terms in the last 2 integrals are the self terms, only present when the test functions are encompassed by the expansion functions. The splitting is obvious in the case of a PEC conductor. The second equation gives us the electric surface currents. Substituting them in the first equation, we obtain the charges. We note that at DC the matrices M_i^r (the only matrices used in the classical EFIE) are zero, which leads to the obvious conclusion that the currents are determined by the incident (tangential) magnetic fields only (through the MFIE), while the charges are determined by the (normal) electric fields. For the general dielectric equations, it is more complex, but we can use the last 2 equations to eliminate or find the charges if the currents are known. We should also not that it is not easy to obtain testing functions appropriate for BOTH charge and currents. We have chosen Dirac test functions, which corresponds with point matching. This leads to a non-square matrices, which are then solved in the least-square sense. The double terms are computed numerically, while analytical expressions for the self terms have been derived [6]. We have also shown that, if the incidents fields satisfy Maxwell's equations, the solution also will [7]. After elimination of the charges, we obtain the following set of simplified but fully stable equations:

$$\begin{bmatrix} \vec{E}_{i,inc} \\ \vec{H}_{i,inc} \end{bmatrix} = \begin{bmatrix} \frac{c_{i+1}^2 M_i^r - \kappa c_i^2 M_{i+1}^r}{\varepsilon_i c_i^2 c_{i+1}^2} & M_i^c - \frac{\varepsilon_{i+1} \kappa M_{i+1}^c}{\varepsilon_i} \\ M_i^c - \frac{\mu_{i+1} \kappa M_{i+1}^c}{\mu_i} & \frac{-c_{i+1}^2 M_i^r + \kappa c_i^2 M_{i+1}^r}{\mu_i c_i^2 c_{i+1}^2} \end{bmatrix} \begin{bmatrix} \vec{J}_{s,e} \\ \vec{J}_{s,\mathrm{m}} \end{bmatrix} \quad (5)$$

with $\kappa = M_i^b (M_{i+1}^{b\ T} M_{i+1}^b)^{-1} M_{i+1}^{b\ T}$. We have now reduced the matrix in (3) to a minimal 3nx3n. Notice that we did not save very much in computer time, since the matrix elements require more than just evaluating the integrals in (4). It should be noted that aggregation methods like the ones used in MLFM (Multilevel Fast Multipole Methods) could also be used to further increase the efficiency. Since those techniques are well known, we will not discuss them here. If one would like to compute the charges, they can always be derived from the currents by the following relations:

$$M_{i+1}^b \begin{bmatrix} -\rho_{s,e} \\ \rho_{s,\mathrm{m}} \end{bmatrix} = \begin{bmatrix} \varepsilon_{i+1}\mu_{i+1} M_{i+1}^r & \varepsilon_{i+1} M_{i+1}^c \\ \mu_{i+1} M_{i+1}^c & -\varepsilon_{i+1}\mu_{i+1} M_{i+1}^r \end{bmatrix} \begin{bmatrix} \vec{J}_{s,e} \\ \vec{J}_{s,\mathrm{m}} \end{bmatrix} \quad (6)$$

The implementation of (5) in a combination of Python and Fortran is the body of STEMO (Stabilized Toolkit for Embedded object MOment Method).

II. EXAMPLES IN THE FREQUENCY DOMAIN

The first checks were made with simple objects like a sphere, where the analytical solution is known (Mie expansion). We notice that is it important to "randomize" the mesh (Fig. 2). Indeed a "too" regular mesh makes it very difficult to represent the currents around the poles of the sphere.

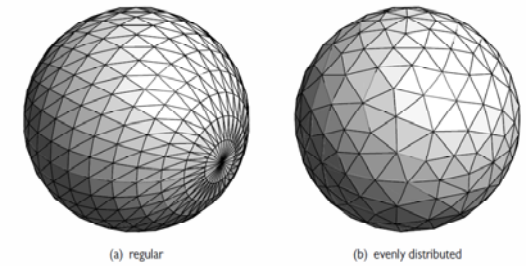

Fig. 2. Regular versus evenly distributed mesh.

The results can be summarized in Table I.

TABLE I: accuracies

(a) surface current

	tangential + normal	tangential	Galerkin
regular	8.19%	5.34%	1.84%
evenly distributed	1.42 %	2.69 %	1.53 %

(b) surface charge

	tangential + normal	tangential	normal
regular	2.27%	120%	2.78%
evenly distributed	0.73%	6.70%	4.78%

We obtain the expected results for a dielectric sphere of 1 m radius at 300 MHz and permittivity 4 (the colours represent the charges and the arrows the size of the currents).

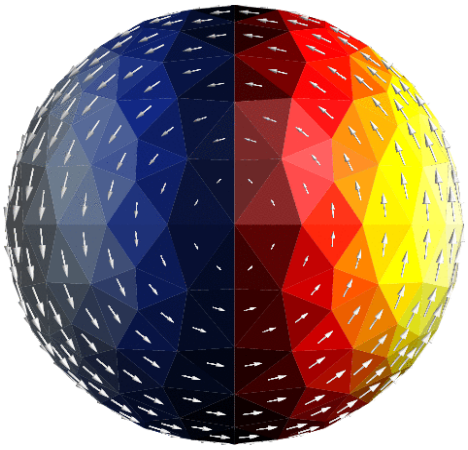

Fig. 3. Charge and current distributions on a dielectric sphere.

More interesting examples are a cube with sharp corners (Fig. 4). We can observe the expected edge behaviour in function of the distance d to the edge [8], namely $d^{-1/3}$ for the currents parallel with the edges and $d^{2/3}$ for the currents perpendicular to the edges.

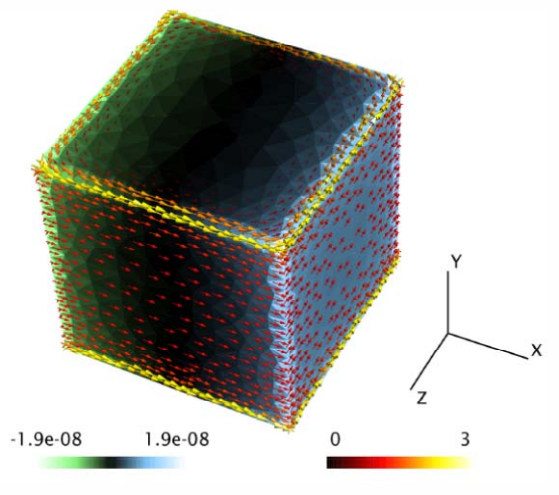

Fig. 4. Charge and current distributions on a dielectric cube with sharp edges at t=0.

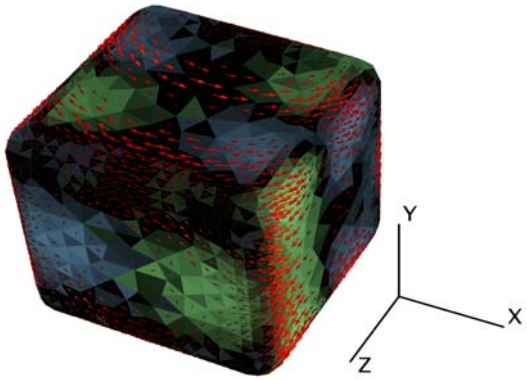

Fig. 5. Charge and current distributions on a dielectric cube with rounded edges at t=T/4.

The case of a rounded corner is more close to the reality, but is easier to compute and never pose any numerical problems since the fields remain finite everywhere (Fig. 5). One just has to make sure that the grids coincide at the edges. More complex shapes, like a torus can do not need this extra effort, since the mesher can handle this object at once (Fig. 6).

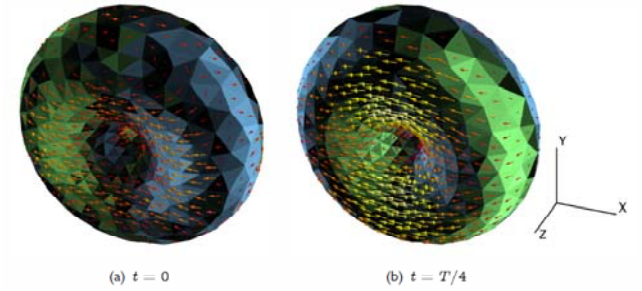

Fig. 6. Charge and current distributions on a torus at different moments in time.

Other examples show the fields in the neighbourhood of a PEC blade of a wind turbine, with different polarisations: One can see, that at large distances, the fields are similar allowing the classical high frequency approximations without modifications. At close distances behind the blades the difference between the case, where the electric field of the incident plane wave is parallel with the longest edge of the blade (Fig. 7) and the case where the field is perpendicular to the blade (Fig. 8), behaves fully like the intuition of an electromagnetic engineer would expect.

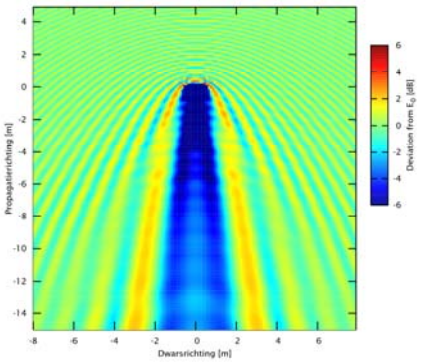

Fig. 7. Field distributions around a PEC turbine blade, parallel polarisation.

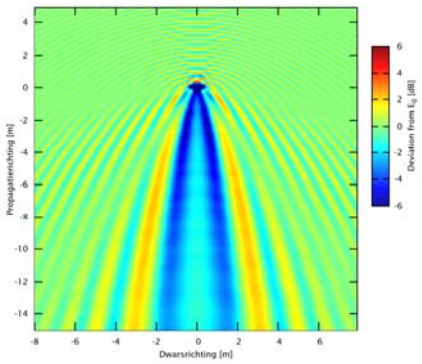

Fig. 8. Field distributions around a PEC turbine blade, perpendicular polarisation.

Also combinations of objects can be easily computed, like 2 dielectric spheres (same as before: 1 m diameter and a permittivity of 4) close to each other (Fig. 9).

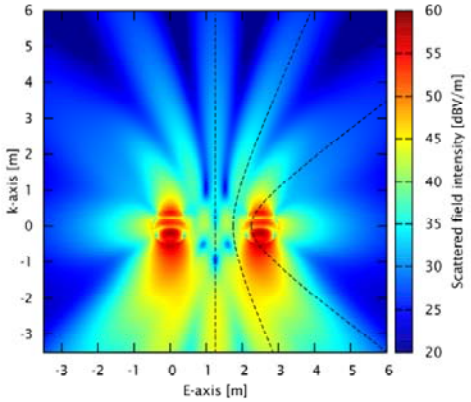

Fig. 9. Field distributions around 2 dielectric spheres.

Even more interesting is to look at the difference between the solution of the solitary sphere compared to the array of 2 spheres (Fig. 10). As expected from the Green's functions the a behaviour far away from each other at nonzero frequency ($1/r^2$) is observed, while at DC the expected ($1/r^4$) is noticed (lowest curve on Fig. 10). Only, when the sphere are nearly touching, a different behaviour is observed.

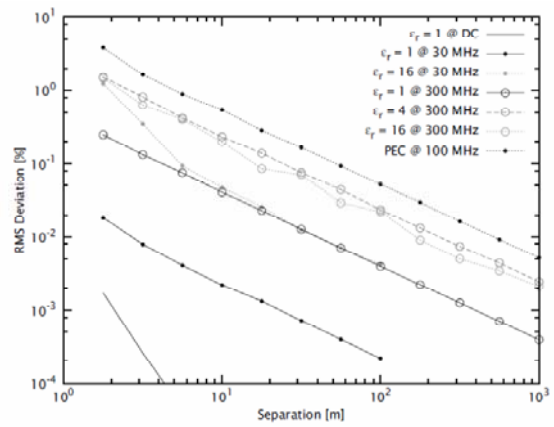

Fig. 10. Field distribution difference on a set of 2 spheres with respect to single one.

A more complex case of a Gaussian beam (up to now plane waves or Hertzian dipoles were used as exciting field) impinging off-centre on a dielectric sphere (diameter 1 m, permittivity 4) is shown in Fig. 11. Here we can see the spreading of the reflected wave and the interference with the incident wave, as well as the focusing of the waves inside the sphere.

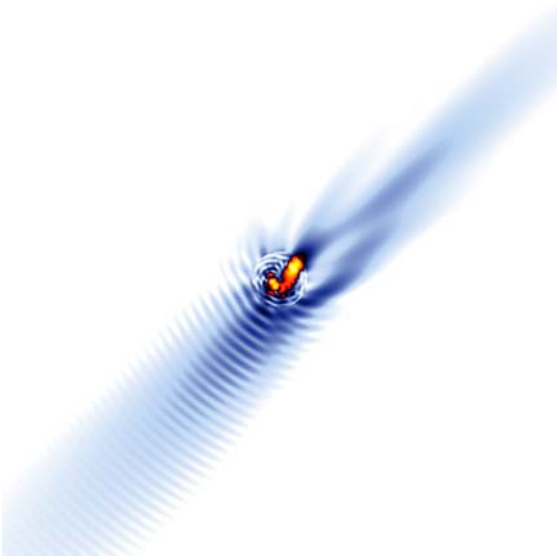

Fig. 11. Field distributions around a dielectric sphere illuminated with a Gaussian beam.

Finally, embedded objects can be easily implemented, even if more complex objects, like a long wire passing through a dielectric sphere would require a lot of extra programming effort. An example is the behaviour of the field lines of a PEC sphere in a sphere with a relative permittivity of 4 at DC(Fig. 12). Up to now, the toolkit is limited to 3 embedded objects, the innermost one being a PEC object.

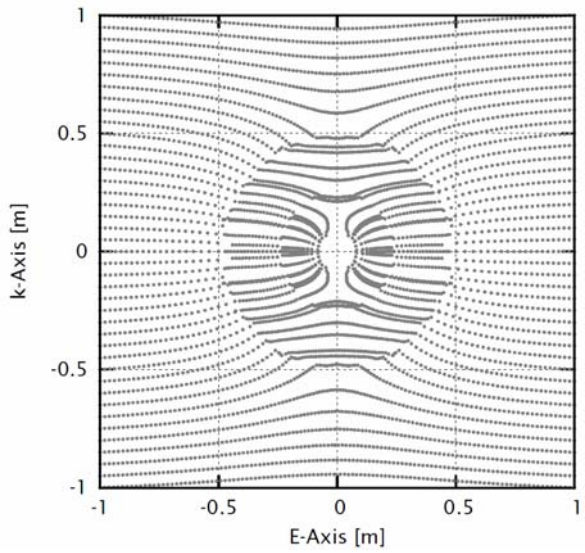

Fig. 12. Field lines around 2 spheres embedded in each other at DC.

III. EXAMPLES IN THE TIME DOMAIN

A nice example is the canonical case of a PEC sphere of 1 m diameter illuminated by a plane wave (Gaussian in the time domain or vertical axis). We can compute and follow the propagation of the wave step by step. In Fig. 13, all time steps are shown at once by the field above and below the sphere by shifting every time slice along a horizontal axis. The computations were performed at 512 frequency points and the FIFT (Fast Inverse Fourier Transform) was used to obtain the fields at a particular moment in time. The main waves (reflected and transmitted behind the sphere) are clearly visible, but also the creeping waves around the sphere, coming indeed much later in time than the main ones.

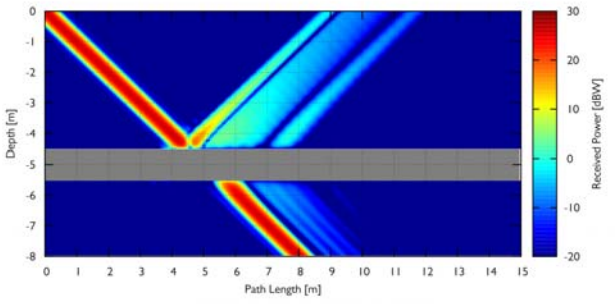

Fig. 13. A PEC sphere illuminated by a plane wave.

The case of a dielectric sphere with a permittivity of 4 but still of 1 m diameter is even more interesting. In Fig. 14, we can even see that the wave is slowed down in the sphere, but that it is caught up by the wave going around the sphere. The inner resonances of the sphere are making the other waves even more pronounced and are the cause of the unexpected fields that are noticed before the arrival of the wave (aliasing effects). This is indeed due to the previous wave, that has still not yet fully faded away, since the basic assumption of the (FI)FT algorithm consists in repeating periodically the under consideration.

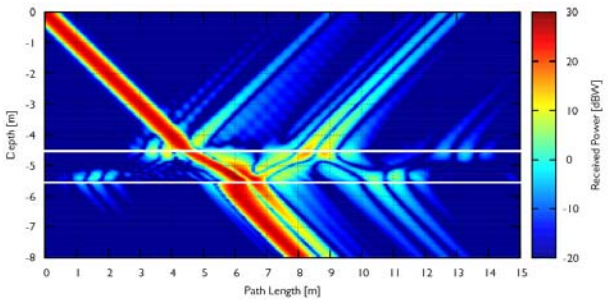

Fig. 14. A dielectric sphere illuminated by a plane wave.

IV. CONCLUSIONS

A toolkit for computing EM fields of generally shaped objects has been produced. It allows to compute many practical problems with an unseen accuracy for objects or the same order of magnitude as the wavelength or smaller (including DC).

ACKNOWLEDGMENT

A large part (70%) of this work has been sponsored by the IWT, the Flemish government agency for Innovation by Science and Technology through a research grant, the rest by consultancy income from industrial projects.

REFERENCES

[1] M. Taskinen and P. Ylä-Oijala, "Current and charge integral equation formulation", Antennas and Propagation, IEEE Transactions on, vol. 54, no. 1, pp. 58–67, Jan. 2006.

[2] W. C. Chew, J.-M. Jin, E. Michielssen, and J. Song,, "Fast and Efficient Algorithms in Computational Electromagnetics", Boston, MA: Artech House, 2001

[3] Van Lil E., De Bleser J. 2014. "On the Accuracy of MoM Solutions for RCS and Propagation Computations". In URSI GASS. Altintas A. (eds.) Beijing, China, 16-23 August 2014 , pp. 1-5

[4] C. Geuzaine and J.-F. Remacle, "Gmsh: a three-dimensional nite element mesh generator with built-in pre- and post-processing facilities", Numerical Methods in Engineering, International Journal for, vol. 79, no. 11, pp. 1309–1331, May 2009.

[5] S. Rao, D. Wilton, and A. Glisson, "Electromagnetic scattering by surfaces of arbitrary shape", Antennas Propagation, IEEE Transaction on, , vol. 30, pp.409–418, May 1982

[6] De Bleser J., Van Lil E., Van de Capelle A. 2011. "A 'Charge and Current' Formulation of the Electric Field Integral Equation", *European Conference on Antennas and Propagation.* Rome, Italy, 11-15 April 2011 , pp. 1-5

[7] De Bleser J., Van Lil E., and Van de Capelle A. 2014. "Split Formulation of the Charge and Current Integral Equations for Arbitrarily-Shaped Dielectrics". Antennas and Propagation. IEEE Transactions on, vol. 62, no. 1, pp. 302-310.

[8] R. Mitra, and, S. W. Lee, Analytical Techniques in the Theory of Guided Waves, p. 10, Macmillan, New York.